We would like to thank the referees for their constructive and valuable criticisms. We have carefully responded to all comments, as reported below.

A preliminary revised manuscript is included in this document.

***The reviewers' comments are in italic text*. Our answers are in normal text.**

Anonymous Referee #1

....

Main remarks =============

- p 1937 lines 20-25. The statement about sigma-coordinate models able to simulate realistic Ekman surface/bottom BL flows is a bit subjective, and too general (in particular these BLs are largely unresolved in this present 12-level implementation). I suggest to drop the part "The POM is a terrain-following... steering"

Done.

- p 1938 lines 1-13. For clarity, I would suggest to reorder the statements in this part. I would suggest to successively describe the geographical domain, the horizontal and vertical resolution, the boundary conditions, the topography (origin, periodization, smoothing), the parameterizations, and integration strategy (duration, time steps). It is not clear whether the zonal and meridional grid steps are proportional to cos(latitude); please clarify (the authors may indicate the meridional resolution in km at the northern and southern boundaries). I suggest to replace the expression "Mercator projection" with "Mercator grid".

The details on eddy-viscosity parameterization, resolution and integration strategy have been postponed after the discussion of the bathymetry. The other suggested corrections have also been made.

- line 14 : replace "drawback" with "limitation". In fact, the whole sentence deserves rewriting (serious style issue). The pressure gradient error is not rigorously due to "complex" but to "steep" topographies. Please recall the mathematical criterion retained to smooth the topography.

The proposed corrections have been made and the mathematical criterion has been recalled.

- line 27 : "process studies".

Done.

- line 29 : is the initial stratification "imposed" (this expression suggest temperature is restored to initial condition throughout the integration) ? Please remove "imposed" if not.

"Imposed" has been deleted.

- p 1939, line 4-5 : what is the structure and strength of the surface heat flux? How is it implemented? Please avoid the somewhat ambiguous word "prescribed" here as well. The expressions "total mixing" and "vertical mixing" are not clear (if not erroneous in this argument). Please be more accurate in the physical argument and expression.

We have rewritten this part and have discussed the structure of the heat fluxes.

- line 10 : I would suggest to replace "is small" with "appears weaker".

Suggestion followed.

- *line 12 : "quite well captured" as compared to which (published) reference?*

We have added the relevant references. Please note that we have replaced the old Fig. 1 with a schematic diagram from Saraceno et al. (2004) and have added a new Fig. 5c that shows the structure of the main ocean current systems in the region of interest. The last two paragraphs of section 2 have been rewritten accordingly.

- *p 1940 line 5 : "quite impressive" is not informative. Please remove and modify the sentence accordingly.*

Done.

- *Section 3: Please present (here or for instance in a subsection 2.2 called "post-processing") the filtering process, and precisely introduce the frequency bands that will be discussed in the rest of the paper. There seems to be 3 bands of interest (at least in the last figure) : low (T>200 days), medium (100-150) and high (0-50) frequency. The depiction of interactions between these various frequency bands would be much more informative (and easy to write and read).*

The filtering performed in section 3 is clearly explained ("The low-frequency signal has been derived by applying a moving average with T=200 days at each grid point"), and the two high-frequency bands introduced in section 5 are clearly defined by the integral in eq. (2), so the three frequency bands have already been precisely defined.

Please avoid confusing sentences, such as line 1 in page 1945 where the 100-160 day period is called "high-frequency" (this band corresponds to 0-50 day elsewhere).

Following this useful comment we have now univocally denoted as "high-frequency range" (HFR) the range 0-50 days and as "intermediate high-frequency range" (IHFR) the range 100-150 days.

Finally, the interval 0-50 day is not valid: if the output archiving frequency were e.g. 5 days, then the 0-50 band should be referred to as "10-50 days".

The smallest scale of the wavelet is 1 day. So, following this useful comment we have stressed this and changed $W_{0,50}$ in $W_{1,50}$ throughout the text.

- *line 21 (and throughout the paper, including figures/captions if needed). The expression "Quasi-climatological state" is not very clear and may be confusing. I would suggest replacing it with e.g. "active state". The whole sentence is confusing as well (the word "thus" is not justified) : please remove this word (or justify it), and split at the end of line 21.*

The expression "quasi-climatological" has been replaced by "active" throughout the text, as suggested by the reviewer. The particular sentence has been modified.

- *p 1941 line 16 : "shorter than T=200 days"*

Corrected.

- *lines 19-22 : Why precisely is this correspondence interesting. Wouldn't one expect to find a minimum (i.e. not a maximum) in variance surrounded by local maxima at the center of Fu et al.'s dipole ?*

The SSH rms shown in Fig. 12 includes all time scales shorter that 200 days and direct reference with the 25-day period oscillation of Fu et al. (2001) is indeed inappropriate. So, following this useful criticism we have removed the sentence.

- *Figs 13 and 14 seem to show the same link between low- and high-frequency signals. Also, it seems that Figs 15 and 16 exhibit similar behaviors. Please consider showing the results either in P2 or in P3 if possible. Also, is it necessary to show 12 (small but crowded) subplots in Figs 9, 15 and 16 ? It seems to me that one sequence of 6 (larger) plots would illustrate the processes discussed in the text.*

Following this useful criticism we have removed the old figures 13 and 15 and presented only one time sequence of the old figure 16 (figure 14 in the revision, which now presents 6 larger plots). We have left figure 9 unchanged because the low-frequency patterns are simpler to see and the two sequences illustrate two relatively different transition properties.

- *page 1942 lines 4-6 : very confusing sentence. Please separate the comments on each period band.*

The sentence has been rewritten.

- *page 1943, line 7 : "generated resonantly" is not clear ; please explain (or remove the word resonantly which does not seem useful).*

"Resonantly" has been removed.

- *lines 21-22 : please remove "in a unique region in this respect". This statement is questionable and not really useful.*

Done.

- *page 1944 line 18 : "main"*

Done.

- *page 1946 line 19 : please replace "temporal" with "frequency".*

Done.

Anonymous Referee #2

....

... the absence of the Brazil Current makes disappear the Brazil-Malvinas Confluence (BMC). As a consequence the mean circulation obtained by the model is somewhat unrealistic. Furthermore, as the BMC region is by far the main factory of eddies in the South Western Atlantic (see Chelton et al 2011 or Saraceno and Provost, 2012), and eddies are believed to drive the circulation around the ZD, comparison of the results with those obtained by other authors that used observations (or included the BMC in their models) is questioned.

Specific comments 1) Figure 5b shows velocity derived from mean SSH from the model. Two very anomalous patters are observed: - Currents over the northern portion of the Patagonian shelf are as intense as the Malvinas Current, which is very unrealistic; - A southward flow parallel to the Malvinas Current could be associated to the Malvinas Return Flow. However it is as intense as the Malvinas Current. According to the figure it looks like this flow is the main source of the ZD anticyclonic circulation. Both features do not correspond to observations. It is most likely that these artifacts are due to the absence of the Brazil Current (BC) coming from the North. It is suggested that a larger domain model, which includes the BC, should be considered to ease the comparison with results from other authors.

The unrealistic currents north of the Patagonian shelf are certainly consequences of the model setup, which does not include the BC, but this was clearly pointed out at page 1939, lines 14-20: "... the Malvinas–Brazil Current Confluence is obviously absent due to the choice of the northern latitude of the domain of integration and of the wind forcing". We also stressed that "...this limitation does not affect our analysis, that is mainly focused on the intrinsic variability of the ZA directly induced by changes of the ACC frontal system, particularly through its Subantarctic Front. This is in fact an innovative aspect of the present study, in which these sources of intrinsic variability can be isolated".

The low latitudes were excluded in the setup because the aim was to analyze the intrinsic variability of (a large portion of) the ACC system. However the referee's suggestion to include the BC is very appropriate, and this extension of the analysis is now explicitly mentioned among the future perspectives in section 6.

2) It will be great to have a map with the RMS of the non filtered SSH obtained by the model. When the BMC is included, the RMS of the non-filtered SSH is maximum at the BMC region and has a relative minimum centered in the ZD region. Saraceno and Provost (2012) show that the latter observation is due to a lower number of eddies in the region isolated by the ZD current. But again, it is difficult to compare with other studies that do have the BMC.

These valuable comments will be taken into account in the future study with an extended domain.

3) Most of the discussion is based on the time series constructed from the two boxes defined in figure 10. Box "B" seems to include a larger portion of the ACC domain than of the ZD domain.

Indeed, but the motivation of this choice is that it turns out to be the best one to characterize the regime shift.

Technical corrections

The manuscript is easy to read. A few sentences could be more precise, but the message is, to my point of view, understandable. Perhaps authors could make an effort to diminish the number of figures.

Following this useful comment (and an analogous comment of referee 1) we have removed the old figures 13 and 15 and presented only one time sequence of the old figure 16 (figure 14 in the revision, which now presents 6 larger plots).

It will help if figures with maps (like figure 5): - Use a geographical projection; - Include the main position of the fronts and - The potential vorticity contours that define the ZD.

Following this useful comment we have added a new Fig. 5c, which is discussed in the last two paragraphs of section 2. To keep the current map easily readable, we did not add potential vorticity contours.

Units are missing in the legend of figure 2. Add latitude and longitude to figure 1.

Units are now added in Fig. 2. The old Fig. 1 has now been replaced with a schematic diagram from Saraceno et al. (2004).

Intrinsic variability of the Antarctic Circumpolar Current System: low- and high-frequency fluctuations of the Argentine Basin flow

G. Sgubin [1], S. Pierini [2] and H. A. Dijkstra [3]

[1]{Laboratoire des Sciences du Climat et de l'Environment, Paris, France}

[2]{Dipartimento di Scienze e Tecnologie, Università di Napoli Parthenope, Napoli, Italy}

[3]{Institute for Marine and Atmospheric research Utrecht, Utrecht University, The Netherlands}

Correspondence to: S. Pierini (stefano.pierini@uniparthenope.it)

Abstract

In this paper, the variability of the Antarctic Circumpolar Current system produced by purely intrinsic nonlinear oceanic mechanisms is studied through a sigma-coordinate ocean model, implemented in a large portion of the Southern Ocean at an eddy-permitting resolution under steady surface heat and momentum fluxes. The mean transport through Drake Passage and the structure of the main Antarctic Circumpolar Current fronts are well reproduced by the model. Intrinsic variability is found to be particularly intense in the Subantarctic Front and in the Argentine Basin, on which further analysis is focused. The low-frequency variability at interannual time scales is related to bimodal behavior of the Zapiola Anticyclone, with transitions between a strong and collapsed anticyclonic circulation in substantial agreement with altimeter observations. Variability on smaller time scales shows clear evidence of topographic Rossby-wave propagation along the eastern and southern flanks of the Zapiola rise and of mesoscale eddies, also in agreement with altimeter observations. The analysis of the relationship between the low- and high-frequency variability suggests possible mechanisms of mutual interaction.

1 Introduction

Ocean model studies of various degrees of complexity forced by steady forcing have suggested in the last two decades that a substantial fraction of the low-frequency variability (LFV) of oceanic frontal structures (ranging from the interannual to the decadal and interdecadal time scales) may be due to highly nonlinear oceanic mechanisms internal to the ocean system: this is the so-called 'intrinsic' LFV variability, that can advantageously be analyzed in the conceptual framework of dynamical systems theory (e.g., see Dijkstra, 2005, and Dijkstra and Ghil, 2005, for reviews). The mechanisms can involve barotropic and baroclinic instability, eddy-mean flow interaction, Rossby wave propagation and interaction with topographic and coastal features. In general, identifying the intrinsic part of the ocean variability, and the modality through which it emerges, is necessary to assess the role played by the ocean in the global climate. In addition, studying these ocean changes is fundamental also from a modeling point of view, as they may not be properly represented even in high-resolution general circulation models due to their high sensitivity to the parameterization of unresolved processes. Most studies have been devoted to the major mid-latitude western boundary currents and of their extensions, such as the Kuroshio (e.g., Qiu and Miao, 2000; Schmeits and Dijkstra, 2001; Pierini, 2006, 2008; Pierini and Dijkstra, 2009; Pierini et al., 2009), the Gulf Stream (e.g., Schmeits and Dijkstra, 2001; Quattrocchi et al., 2012), and the Agulhas Current (e.g., Dijkstra and De Ruijter, 2001; Le Bars et al., 2012).

A good candidate for considerable intrinsic LFV is also the Antarctic Circumpolar Current (ACC) system (e.g., Rintoul et al., 2001) and its complex frontal structure in the Southern Ocean. The ACC plays an important role in the global climate through local water mass formation, ocean carbon sequestration and heat storage, and because of its ability to connect climate signals at all longitudes. Hogg and Blundell (2006) analyzed the LFV of the ACC by using an idealized multi-layer quasi-geostrophic model forced by steady winds. Their simulations display robust intrinsic LFV, which is shown to involve a positive feedback between baroclinic eddies and the mean circulation. Penduff et al. (2011) analyzed the sea level expression of intrinsic LFV in simulations of an eddy-permitting Ocean General Circulation Model (OGCM), and found their results in the Southern Ocean to be basically consistent with those of Hogg and Blundell (2006). O'Kane et al. (2013) used an OGCM (including sea ice) to identify a Southern Ocean southeast Pacific mode of intrinsic LFV through a suite of experiments that include low-frequency (ENSO, SAM) and high-frequency stochastic forcing. Giarolla and Matano (2013) used long time series of sea surface height (SSH), sea surface temperature and wind stress curl to determine the main modes of LFV of the Southern Ocean circulation, but they did not investigate its intrinsic component.

An oceanic region particularly relevant for climate that affects the Southern Ocean dynamics, and where important LFV was documented, is the Argentine Basin (AB), located in the South Atlantic sector near the South American coast. The AB is a crucial region where strongly contrasted water masses meet and mix (Fig. 1), and where the circulation is likely to influence meridional water exchanges between the Southern Ocean and subtropical latitudes (Piola and Gordon, 1989) with associated strong impact on the global climate system. An intense barotropic anticylonic circulation called Zapiola Anticyclone (ZA) was documented over the Zapiola Rise (ZR), a high sedimentary deposit located in the middle of the AB (Weatherly, 1993; Whitworth et al., 1991; Saunders and King, 1995). The ZA affects considerably the surface exchanges between the ACC and the South Atlantic Current (Smythe-Wright and Boswell, 1998) and is supposed to contribute to determine global deep water mass characteristics (Garzoli et al., 2008).

The ACC dominates the southern part of the basin, splitting into two major fronts, the Polar Front and the Subantarctic Front (Fig. 1). The latter flows northwards after leaving the Drake Passage, forming the Malvinas Current which transports cold and relatively fresh subantarctic waters equatorward. Its return flow eventually aligns with the southern edge of the ZR and represents the local manifestation of the Subantarctic Front. This front and the Polar Front join at around (49°S,45°W) and diverge further east. From the north, the warm and salty Brazil Current flows southward along the continental shelf, colliding with the Malvinas Current at around 38°S, where the very energetic and turbulent region known as the Malvinas-Brazil Current Confluence is created.

Significant LFV of the ZA was observed with in situ (Hughes, et al., 2007) and altimeter data (Saraceno et al., 2009). Saraceno et al. (2009) documented for the first time that the ZA flow may significantly decrease in strength or even vanish over an interannual time scale, with a cyclonic pattern emerging from time to time. Bigorre and Dewar (2009) developed an idealized quasi-geostrophic ocean process study about the circulation around a large scale topographic anomaly: the role of bottom friction and eddy diffusivity was found to be consistent with the theory proposed by Dewar (1998) for the mean flow, moreover the modeled LFV was shown to bear important similarities to that observed. Venaille et al. (2011) found intrinsic high- and low-frequency variability of the ZA in their comprehensive ocean model, and explained the internal part as the result of an eddy-driven stochastic process. In the same basin also high-frequency fluctuations were observed (Fu et al., 2001; Tai and Fu, 2005), and were interpreted in terms of topographic Rossby modes (Weijer et al., 2007a,b) and mesoscale variability (Fu, 2007).

In this paper, a model study aimed at identifying and analyzing the intrinsic variability of the ACC system, with a focus on its Subantarctic Front and relative effect on the AB flow, is presented. A primitive equation sigma-coordinate ocean model is implemented in a large portion of the Southern Ocean with an eddy-permitting resolution under steady forcing; the climatological forcing and the stratification are substantially idealized, while the topography (that plays a fundamental role at these high latitudes) is represented in more detail (Sect. 2). In Sect. 3 the LFV of the model flows is analyzed, with an emphasis on the AB where the highest level of variance is found. Regime switches occurring on interannual time scales of the AB flow are found to share important similarities with the long-term variations of the ZA as observed by Saraceno et al. (2009). In Sect. 4 the intrinsic high-frequency variability (HFV) in the AB, emerging as a residual from the LFV, is analyzed through a wavelet analysis and interpreted in terms of topographic Rossby waves and mesoscale eddies. In Sect. 5 the relation between the LFV and the HFV is analyzed by introducing dynamical indices, and possible mechanisms of mutual interaction are suggested. Finally, in Sect. 6 conclusions are drawn.

2 The model

The model used in this work (Sgubin, 2012) is the Princeton Ocean Model (POM) developed by Blumberg and Mellor in 1977 and subsequently improved and updated (for general information see www.aos.princeton.edu/WWWPUBLIC/htdocs.pom/). POM is a primitive equation sigma-coordinate model that contains a turbulence sub-model for vertical mixing based on the Mellor-Yamada scheme (Mellor and Yamada, 1982). Details of the model equations and numerical solution techniques can be found in the POM Users Guide (Mellor, 2003). The quantitative success of the ZA circulation model of de Miranda et al. (1999) was attributed to the use of this kind of vertical discretization (see also Barnier et al., 2006, for relevant modeling issues).

The model domain includes Pacific and Atlantic sectors of the Southern Ocean, extending meridionally from 33.2°S to 72°S and longitudinally from 120°W to 0°W (Fig. 2). Periodic boundary conditions along the eastern and western meridional boundaries are imposed with a 12° transition region (with 10° to the west and 2° to the east; in that region the bathymetry is interpolated so as to match at the two boundaries). On the northern and southern boundaries free-slip boundary conditions are imposed at all depths.

The Mercator grid is adopted with the ETOPO5 bathymetry data (available online at http://www.ngdc.noaa.gov/) on a grid with a horizontal spatial resolution of 1/5° in latitude

($\sim 22\ km$) and 2/5° in longitude ($\sim 13.75 - 37.2\ km$). A limitation of sigma-coordinate models is related to the existence of pressure gradient errors that arise when computing the horizontal pressure gradient near a steep topography (e.g., Haney, 1991; Beckmann and Haidvogel, 1993). This error is caused by large numerical truncations in the transformation from the z-coordinate to the sigma-coordinate. A reduction of such errors to acceptable values can be achieved by properly smoothing the bathymetry according to a criterion involving the bottom slope and the horizontal and vertical grid resolution. At the same time, such smoothing should retain the main features of the topography in order to consistently reproduce the interactions between the flow and the oceanic bottom, and should avoid hydrostatic inconsistency. This problem was successfully handled by Barnier et al. (1998), Marchesiello et al. (1998) and de Miranda et al. (1999) in setting up a consistent model for the South Atlantic circulation. We have therefore applied the method of Barnier et al. (1998) to obtain a model topography that reduces drastically the pressure gradient error. The method imposes an upper bound on the maximum relative variation r_h of the model ocean depth, defined as:

$$r_h(i,j) = \frac{2max[|h(i+1,j) - h(i,j)|, |h(i,j+1) - h(i,j)|]}{min[|h(i+1,j) + h(i,j)|, |h(i,j+1) + h(i,j)|]}$$

where h is the local water depth. By imposing $r_h < 0.3$ the error has been reduced by two orders of magnitude compared to the unsmoothed topography case. Furthermore, in order to avoid hydrostatic inconsistency related to the vertical integration scheme, the maximum relative increase in bottom topography must be less than the distance between two consecutive sigma-levels (Barnier et al., 1998). We have thus performed a further smoothing to satisfy this requirement for every vertical level.

The Smagorinsky parameterization has been used for the horizontal eddy viscosity with the dimensionless HORCON parameter (Mellor, 2003) $H = 0.12$. The model has 12 vertical sigma levels and is integrated for 80 years from motionless initial conditions with external and internal time steps $\Delta t_e = 20\ s$ and $\Delta t_i = 600\ s$, respectively. Following the approach typical of process studies of the intrinsic LFV, an idealized but relatively realistic steady zonal wind stress field is used: Fig. 3a shows the wind stress profile based on the Trenberth et al. (1989) climatology. The initial stratification, again idealized but relatively realistic, is shown in Fig. 3b for the temperature (the salinity has been held constant): it takes into account the vertical as well as the meridional density gradient, which effectively influences the zonal flow at Drake Passage. In order to sustain such a stratification, idealized steady surface heat fluxes have been imposed: their spatial structure (varying sinusoidally in latitude) has been empirically evaluated so that the initial stratification is not significantly altered during the simulations.

Fig. 4 shows the volume transport through the Drake Passage: the average value of ~116 Sv is in reasonable agreement with the real estimated value of ~130 Sv (e.g., Rintoul et al., 2001); an energetic HFV is present in the signal while the LFV in this integrated parameter appears weaker. Figs. 5a,b show the temporal means of the SSH η and of the depth-integrated current $\mathbf{u}$, respectively. Fig. 5c is a zoom of Fig. 5b limited to the southwestern Atlantic (one arrow out of 6 is drawn). The position and structure of the local ACC branches, i.e. those associated with the Polar Front and the Malvinas Current are quite well captured by the model (e.g., Rintoul et al., 2001; Saraceno et al., 2004, compare with Fig. 1 from that paper). The ZA has the correct shape and location, being centered at ~(315°E,45°S). The Polar and Subantarctic fronts meet correctly at around 50°S just east of 45°W, and diverge further east (see Fig. 5b), as in the real ocean.

The Brazil Current and the Subtropical Front (located at around 39°S) associated with the Malvinas-Brazil Current Confluence are absent due to the choice of the northern latitude of the domain of integration and of the wind forcing. Thus, the flow along the southern American coast is unrealistic north of around 40°S. However, this limitation does not affect our analysis, that is mainly focused on the intrinsic variability of the ZA directly induced by changes of the ACC frontal system, particularly through its Subantarctic Front (this is in fact an innovative aspect of the present study, in which these sources of intrinsic variability can be isolated). Thus, the branch of the Subantarctic Front indicated by the red arrow in Fig. 5c does not derive from the Malvinas return flow (which is absent for the same reason discussed above), but from a southward current which, mainly because of topographic interactions, acquires nonetheless the correct shape and location.

3 Intrinsic low-frequency variability

In this section the LFV produced by the model is presented and discussed. The low-frequency signal has been derived by applying a moving average with $T = 200\ days$ at each grid point. The decimal logarithm of the resulting rms of the SSH is shown in Fig. 6. Apart from a moderate variability in regions of strong topographic variations between ~230-260°E and 345-360°E, a very intense LFV is present all along the Subantarctic Front between ~302-345°E. The particularly intense variability across the southern topographic limits of the AB is consistent with the findings of Saraceno et al. (2009).

The analysis will therefore be focused on this region. Fig. 7b shows the time series of the SSH taken at point P1 where the variability is maximum (see Fig. 7a), which is ~2° south of the ZA center. The behavior yields a chaotic vacillation of O(1 *m*) that has a bimodal character: a detailed analysis will be carried out within the 10-year reference interval delimited by the red lines of Fig. 7b.

Fig. 8 shows the SSH (total signal η: black line; low-frequency signal $\tilde{\eta}$: blue line) at P1 during the reference interval; the SSH maps in the AB corresponding to the two sequences of six instants denoted by the green and red dots in Fig. 8 are shown in Fig. 9. In sequence (a) a well-defined ZA centered at (315°E,46°S) is present at *t*=24600 *days*, corresponding to a SSH maximum at P1, but one year before (*t*=24200 *days*) and after (*t*=25000 *days*) the anticyclonic circulation is weaker and shifted westward by 2-5°, while a cyclonic circulation moving from south-east intensifies and takes its place. Sequence (b) shows an abrupt transition from a collapsed but quite variable ZA (*t*=26200-26600 *days*) to an intense ZA (*t*=27000-27200 *days*). These transitions from a quasi-climatological state of the ZA (denoted as "active state" heretofore) to a collapsed ZA (and vice-versa) are very similar to the variations of the ZA documented by Saraceno et al. (2009). The hypothesis is therefore that the oceanic intrinsic variability plays an important role in this phenomenon.

The preceding analysis has shown that a ZA in an active state is characterized by large values of $\tilde{\eta}$ at P1 ($\tilde{\eta} \approx 1\ m$) while, for a collapsed ZA, $\tilde{\eta} \approx 0 - 0.3\ m$: to this respect, Fig. 7b may provide qualitative information on the character and statistics of the transitions. However, $\tilde{\eta}$ gives only very local information and is not necessarily indicative of a circulation regime. A better way to characterize the ZA state is to rely on the (dimensionless) relative vorticity ζ (and of its low-frequency version $\tilde{\zeta}$) averaged over specific regions of the AB. The two maps of Fig. 10 show $\tilde{\zeta}$ in a collapsed (*t*=25000 *days*) and active state (*t*=27200 *days*): it is evident that the two sectors A and B can very efficiently characterize the ZA state in terms of $\tilde{\zeta}$ averaged in each of them.

The graph of Fig. 10 shows $\langle\zeta\rangle_A$ (red line) and $\langle\zeta\rangle_B$ (blue line) as a function of time for the reference interval: as could be expected, in a collapsed state $\langle\zeta\rangle_A > 0$ and $\langle\zeta\rangle_B < 0$ whereas for a active state both parameters are positive, with a tendency of $\langle\zeta\rangle_B$ to be greater. Fig. 11 shows the scatter plot of $\langle\tilde{\zeta}\rangle_B$ versus $\langle\tilde{\zeta}\rangle_A$ for the whole 80 *yr* integration: the active state is represented by the compact cluster with $\langle\tilde{\zeta}\rangle_B > 0$ while the collapsed state with $\langle\tilde{\zeta}\rangle_B < 0$ is represented by a more diffuse cluster, which implies that this state cannot be characterized by a well defined circulation pattern, as is the case for the active state. Moreover, the abrupt character of the transitions is clearly shown by the small number of dots in the intermediate range. Possible mechanisms that govern this LFV will be discussed in Sect. 5.

4 Intrinsic high-frequency variability

In this section the high-frequency component of the intrinsic variability is analyzed, while its relation with the LFV will be considered in the next section. The high-frequency components is defined here in terms of the SSH as the residual $\eta' = \eta - \tilde{\eta}$, and therefore includes periods shorter than $T = 200\ days$. Fig. 12 shows the rms of η' in the AB: a region of intense variability crosses the isobaths from the deep sea just off the continental shelf in the south-west side of the ZR, reaching the peak of the ZR itself, and presents two maxima at P2=(313°E,47°S) and P3=(317°E,45.5°S).

Fig.s 13a shows the time series of η' (red line) and $\tilde{\eta}$ (blue line) at P3. The HFV has a very intermittent behavior and yields an apparent relation with the LFV, in that the high frequency is more energetic in the collapsed state, corresponding to low values of $\tilde{\eta}$. Because of the intermittency of the HFV (also found in altimeter data by Tai and Fu, 2005, and Fu, 2007), a spectral analysis can most appropriately be carried out by means of the continuous wavelet transform (e.g., Torrence and Compo, 1998). Fig.s 13b shows the amplitude $w(s,t)$ of the corresponding wavelet transform of η, where s is the time scale (only the scales $s \leq 200\ days$ are shown). The period band $0 - 50\ days$ includes topographic Rossby waves and modes (Fu et al., 2001): here the amplitude is reduced and very intermittent over time scales ranging from 100 to 300 *days* (in agreement with Fu, 2007). In the period band $100 - 150\ days$ the amplitude is higher and less intermittent, but is often clearly related to the higher frequency variability (also this is consistent with the results of Fu, 2007, but see the next section for a more careful comparison).

For a qualitative analysis of the flow patterns of the HFV, a sequence of snapshots of the SSH residual η' is reported in Fig. 14. The 25-*day* long sequence is sampled every 5 *days* and corresponds to a maximum in the wavelet amplitude at P3 in the period band $0 - 50\ days$ (see the oval in Fig. 13b). Very complex patterns arise, with length scales ranging from O(1°) or less for the mesoscale up to O(5°-10°) for topographic Rossby waves. The variability is mainly confined over the ZR and shows a clear propagation of features originating from the south-western side of the ZR itself. A wave train follows the southern limits of the rise and turns counterclockwise along its eastern flank: in doing so the vortices undergo substantial stretching and deformation. These waves can be interpreted as topographic Rossby modes (Fu et al., 2001; Tai and Fu, 2005; Weijer et al., 2007a,b). The patterns appear more complex than those typically shown in this location by altimeter data after high-pass filtering the motions with time scales longer than ~1 month (e.g., Fu et al., 2001). This is because our high-frequency signal contains also the longer-term variability associated with the mesoscale eddy field.

A general feature that deserves to be emphasized is the varying length scale of the vortices, that is smaller in the south-west side of the ZR and tends to increase as the pattern propagates. This transition from the mesoscale to the Rossby mode scale is compatible with the energy exchange found to be at work in this region by Fu (2007): this aspect will be analyzed in more detail in the next section. From this qualitative analysis it appears that the topographic Rossby modes in the ZR are not necessarily generated directly by the wind forcing, but may also be of intrinsic origin. Presumably this happens through low-frequency fluctuations of the local circulation (e.g., see Pierini, 1996), that in this case are intrinsic. This also supports the hypothesis that the wind-generated topographic Rossby modes may as well be generated through the same mechanism, in which case the current fluctuations that produce them are not intrinsic but directly wind-driven (e.g., Pierini et al., 2002; see section 5.3 for further discussion).

5 Relation between low- and high-frequency variability

In the Sections 3 and 4 we have identified intrinsic LFV on interannual time scales yielding regime switches from an active ZA to a collapsed ZA, but HFV was found as well. A high-frequency range (HFR, $0-50\ days$) includes topographic Rossby modes; the behaviour in an intermediate high-frequency range (IHFR, $100-150\ days$) appears to be related to that of the HFR. Now, a question arises: is there a relation between these three forms of intrinsic variability in our model results? In general, analyzing this issue is fundamental from a theoretical viewpoint, as it could shed light into dynamical mechanisms that involve a wide range of spatial and temporal scales.

A preliminary qualitative analysis of this kind is presented here. First of all we define a Zapiola index as follows:

$$Z = \langle\tilde{\zeta}\rangle_A - \langle\tilde{\zeta}\rangle_B \qquad (1)$$

The graph of Fig. 10 shows $\langle\zeta\rangle_A$ and $\langle\zeta\rangle_B$ for the reference interval: the two signals are virtually in counterphase in a ZA collapsed state while they tend to be both positive in an active ZA state, with the second signal being higher. Thus, Z as defined in (1) (and shown by the green line in Fig. 15 for the reference interval) is a good global low-frequency indicator of the ZA state, for which a large positive value implies a collapsed state, while a negative or small positive value implies an active state. To construct high-frequency indices we can define the integral of the wavelet amplitude at the reference point P3 within two time scales:

$$W_{s_1,s_2}(t) = \int_{s_1}^{s_2} w_{P_3}(s,t)ds \qquad (2)$$

Thus, the two indices $W_{1,50}$ ($s = 1\ day$ is the smallest scale of the wavelet transform) and $W_{100,150}$ (red and blue lines of Fig. 15, respectively) are good indicators of the behavior in the HFR and IHFR, respectively. We pass to discuss three possible interactions suggested by Fig. 15 and by other experimental and numerical investigations.

5.1 Relation between $W_{100,150}$ and Z

Several works (e.g., Dewar, 1998; Bigorre, 2005; Bigorre and Dewar, 2009; Volkov and Fu, 2008; Venaille et al., 2011, Saraceno and Provost, 2012) have suggested that the mesoscale eddy activity provides the main source of energy of the ZA. By studying the correlation between the eddy kinetic energy and the LFV of the ZA with 15 years of altimeter records, Saraceno et al. (2009) found support of that hypothesis, suggesting a rapid adjustment of the ZA to changes in the eddy kinetic energy. By using high-resolution altimeter data produced by the Archiving, Validation and Interpretation of Satellite Oceanographic data (AVISO) project, Fu (2007) found that the variance-preserving spectrum of the mesoscale energy time series in the AB is spread over a wide range of frequencies, with the majority in the seasonal-to-interannual range, but a significant variance is present also in the range 100-160 days (basically our IHFR): thus, $W_{100,150}$ represents a good index for the high frequency mesoscale in the AB.

In our model results, both transitions present in the reference interval from a collapsed to an active ZA (occurring at $t \approx 24400, 26700\ days$ when Z decreases abruptly, Fig. 15) are preceded by a large $W_{100,150}$, which decreases as the transition to the active state is occurring, with a lag of 100-300 *days* between the two signals. Moreover, the collapse of the ZA at $t \approx 24700\ days$ is followed by an increase of $W_{100,150}$ with a lag of ~200 *days*. This behavior is compatible with a transfer of energy from the eddy field to the large scale circulation during the collapsed ZA - active ZA transition, and vice-versa, and therefore appears to be in basic agreement with the theoretical and experimental arguments reported above: it is interesting to note that purely intrinsic oceanic mechanisms are able to produce such a dynamical process.

5.2 Relation between $W_{1,50}$ and $W_{100,150}$

Using altimeter observations, Fu (2007) analyzed the possible relationship between the 25-*day* barotropic Rossby waves and the energetic baroclinic mesoscale eddies in the ZA region. The wave amplitude was found to be coherent with the energy of the high-frequency mesoscale variability, in that when the latter decreases the wave amplitude increases and vice-versa, suggesting an exchange of energy between the two scales. An indication of this behavior in our model results (for which changes in the wave amplitude and in the mesoscale eddy field are represented by $W_{1,50}$ and $W_{100,150}$, respectively) can be found in the intervals $t \approx 23800 - 24700\ days$ and $t \approx 25900 - 26400\ days$ (Fig. 15), which both precede the transition from a collapsed to an active ZA state. The latter property is particularly interesting, as it suggests a relationship between the energy exchange in the high-frequency ranges and the large-scale LFV of the ZA that deserves to be analyzed in future studies.

5.3 Relation between $W_{1,50}$ and Z

During the transition from an active to a collapsed ZA in the interval $t \approx 24600 - 25000\ days$ no relationship such as the one described above seems to exist between $W_{1,50}$ and $W_{100,150}$; on the other hand, the sudden increase of the energy level in $W_{1,50}$ follows the abrupt collapse of the ZA. This suggests that an impulsive generation of topographic Rossby modes can be active, perhaps with the involvement of mesoscale eddies as discussed at the end of Sect. 4. To this respect, laboratory experiments in a rotating tank performed by Pierini et al. (2002) confirmed the hypothesis put forward in a previous numerical study on topographic Rossby modes in the Strait of Sicily (Pierini, 1996), according to which topographic Rossby modes can effectively be excited by rapid changes of the mean flow (provided in the tank by the movement of a large paddle). In a Rossby mode the time scale is set by the bottom topography and coastlines (if present) and not by the spectral content of the wind field, which only indirectly forces the modes through changes in the mean flow. This may explain why Fu et al. (2001) did not find any significant wind variability at periods close to 25 days in the AB, nor could they find any significant correlation between the variability of the wave amplitude with the variability of the wind stress curl. Thus, the impulsive generation of topographic Rossby modes, which appears to be active in our numerical results, should be considered when explaining the variability in our HFR.

It is clear that understanding the intricate mutual interaction among these three different temporal scales requires a much deeper investigation than that presented in this analysis, which cannot by itself determine any causality between the various scales. Nonetheless, these results can complement those quoted above for future, more advanced investigations in this very peculiar and interesting oceanic site.

6 Conclusions

In this paper, an eddy-permitting sigma-coordinate ocean model has been applied to a large portion of the Southern Ocean with the aim of identifying and analyzing low- and high-frequency fluctuations of intrinsic oceanic origin - a fundamental task for understanding the role of the ocean in the global climate. The approach is typical of process-oriented studies of the intrinsic oceanic variability (idealized but relatively realistic steady winds and stratification), but a realistic topography is used because barotropic motions, and so topographic interactions, are important here. The obtained mean flow is in good agreement with observations as far as the transport through the Drake Passage and the structure of the main Antarctic Circumpolar Current fronts are concerned. Important variability of both low- and high-frequency nature is found, being particularly intense in the branch of the Subantarctic Front corresponding to the Argentine Basin, which, due to its crucial location plays an active role in determining the circulation in the south-west Atlantic sector of the Southern Ocean. The variability over interannual time scales shows a bimodal behavior of the Zapiola Anticyclone, connecting an active state to a state in which the anticyclonic circulation collapses and sometimes reverses locally: this is in substantial agreement with the altimeter observations of Saraceno et al. (2009). The high-frequency residual signal shows clear evidence of mesoscale propagating patterns particularly along the southern flanks of the Zapiola Rise, and a counterclockwise rotation of larger scale topographic Rossby modes over the rise, in substantial agreement with observations. Thus, the main conclusion is that these forms of variability are compatible with intrinsic generation mechanisms all internal to the ocean system. A preliminary analysis of the mutual relationship between the low-frequency variability and two components of the high-frequency variability puts in evidence interesting agreement with observations and previous theoretical and modeling studies, and at the same time suggests a deeper analysis of the results.

Future perspectives include new simulations using a domain with a larger latitudinal extension, so as to represent the Brazil Current and the Malvinas-Brazil Current Confluence. This will allow us to directly compare the modeled eddy field in the southwestern Atlantic with that observed from altimeter data (e.g., Saraceno and Provost, 2012) and to assess its contribution to the low-frequency variability of the Zapiola Anticyclone. Other studies will be devoted to analyzing the sensitivity of the model response to changes in the forcing and parameterizations. For example, changing the amplitude of the wind forcing and/or the parameterization of dissipative effects can produce important modifications in the intrinsic variability (e.g., see the analysis of Pierini et al., 2009, in the context of the Kuroshio Extension bimodality). Another fundamental aspect that should be analyzed is the effect of time-dependent forcing on the emergence of the intrinsic oceanic variability. The intrinsic variability is often in the form of relaxation oscillations that are self-sustained beyond a given tipping point (global bifurcation in some state space) associated with a particular control parameter, while they do not emerge below that threshold under steady forcing (e.g., Simonnet et al., 2005). However, the same intrinsic relaxation oscillations can emerge even below the bifurcation point provided an appropriate noise (e.g., Sura, 2001; Frankcombe et al., 2009; Pierini, 2010; 2012), a deterministic time-dependent component (e.g., Otterå et al., 2010; Crucifix, 2012; Pierini, 2014) or both (e.g., Pierini 2011) are added to the forcing. Thus, using steady forcing, as done here, constitutes only the first step toward the identification of the intrinsic variability: further studies that include both wind noise and the main modes of atmospheric variability in the Southern Ocean will have to be carried out.

Acknowledgments

This research was supported by the MATH-ACC Project funded by the Italian "Programma Nazionale di Ricerche in Antartide" (PNRA Contract n. 2010/A2.11-2753). The work of HD was also sponsored by the COMPLEXITY Project PreKurs funded by the Netherlands Organization for Scientific Research (NWO). We would like to thank two anonymous reviewers, whose detailed comments helped improve the manuscript.

References

Barnier, B., Marchesiello, P., de Miranda, A. P., Molines, J.-M., and Coulibaly, M.: A sigma-coordinate primitive equation model for studying the circulation in the South Atlantic. part I: Model configuration with error estimates, Deep-Sea Res., 45, 543-572, 1998.

Barnier, B., and collaborators: Impact of partial steps and momentum advection schemes in a global ocean circulation model at eddy permitting resolution, Ocean Dyn., 56, 543-567, 2006.

Beckmann, A., and Haidvogel, D.: Numerical simulation of flow around a tall isolated seamount. part I: Problem formulation and model accuracy, J. Phys. Oceanogr., 23, 1736-1753, 1993.

Bigorre, S.: Topographic effects on wind driven oceanic circulation, Ph.D. Thesis, Florida State University, 100 pp., 2005

Bigorre, S., and Dewar, W. K.,: Oceanic time variability near a large scale topographic circulation, Ocean Mod., 29, 176-188, 2009.

Crucifix, M.: Oscillators and relaxation phenomena in Pleistocene climate theory, Philos. Trans. Roy. Soc. London, A370, 1140-1165, 2012.

De Miranda, A. P., Barnier, B., and Dewar, W. K.: On the dynamics of the Zapiola Anticyclone, J. Geophys. Res., 104, 21139-21149, 1999.

Dewar, W. K.: Topography and barotropic transport control by bottom friction, J. Mar. Res., 56, 295-328, 1998.

Dijkstra, H. A.: Nonlinear Physical Oceanography, Springer, 532 pp., 2005.

Dijkstra, H. A., and de Ruijter, W. P. M.: On the physics of the Agulhas Current: steady retroflection regimes, J. Phys. Oceanogr., 31, 2971-2985, 2001.

Dijkstra, H. A., and Ghil, M.: Low-frequency variability of the large-scale ocean circulation: A dinamical systems approach, Rev. Geophys., 43, RG3002, 2005.

Frankcombe, L. M., Dijkstra, H. A., and Von der Heydt, A. S.: Noise induced multidecadal variability in the North Atlantic: excitation of normal modes. J. Phys. Oceanogr., 39, 220-233, 2009.

Fu, L.-L.: Interaction of mesoscale variability with large-scale waves in the Argentine Basin, J. Phys. Oceanogr., 37, 787-793, 2007.

Fu, L.-L., Cheng, B., and Qiu, B.: 25-day period large-scale oscillations in the Argentine Basin revealed by the TOPEX/Poseidon altimeter, J. Phys. Oceanogr., 31, 506-517, 2001.

Garzoli, S. L., Piola, A. R., Speich, S., Baringer, M., Goni, G., Donohue, K., Meinen, C., Matano, R. P.: A monitoring system for heat and mass transports in the South Atlantic as a component of the meridional overturning circulation, Workshop Report: Estancia San Ceferino, Buenos Aires, Argentina, 8–10 May 2007, 38pp, International CLIVAR Project Office, Southampton, UK, 2008.

Giarolla, E., and Matano, R. P.: The low-frequency variability of the Southern Ocean circulation, J. Climate, 26, 6081-6091, 2013.

Haney, R. L.: On the pressure gradient force over steep topography in sigma coordinate ocean models, J. Phys. Oceanogr., 21, 610-619, 1991.

Hogg, A. M., and Blundell, J. R.: Interdecadal variability of the Southern Ocean, J. Phys. Oceanogr., 36, 1626-1645, 2006.

Hughes, C. W., Stepanov, V. N., Fu, L.-L., Barnier, B., and Hargreaves, G. W.: Three forms of variability in Argentine Basin ocean bottom pressure, J. Geophys. Res., 112, C01011, 2007.

Le Bars, D., de Ruijter, W. P. M., and Dijkstra, H. A.: A new regime of the Agulhas Current retroflection: turbulent choking of Indian-Atlantic leakage, J. Phys. Oceanogr., 42, 1158-1172, 2012.

Marchesiello, P., Barnier, B., and de Miranda, A. P.: A sigma-coordinate primitive equation model for studying the circulation in the South Atlantic. part II: Meridional transport and seasonal variability, Deep-Sea Res., 45, 573-608, 1998.

Mellor, G. L.: Users guide for a three-dimensional, primitive equation, numerical ocean model, Prog. in Atmos. and Ocean Sci., Princeton University, 53 pp., 2003.

Mellor, G. L., and Yamada, T.: Development of a turbulence closure model for geophysical fluid problems, Rev. Geophys. Space Phys., 20, 851-875, 1982.

O'Kane, T. J., Matear, R. J., Chamberlain, M. A., Risbey, J. S., Sloyan, B. M., and Horenko, I.: Decadal variability in an OGCM Southern Ocean: intrinsic modes, forced modes and metastable states, Ocean Mod., 69, 1-21, 2013.

Otterå, O. H., Bentsen, M., Drange, H., and Suo, L.: External forcing as a metronome for Atlantic multidecadal variability, Nat. Geosci., 3, 688-694, 2010.

Penduff, T., Juza, M., Barnier, B., Zica, J., Dewar, W. K., Treguier, A.-M., Molines, J.-M., and Audiffren, N.: Sea level expression of intrinsic and forced ocean variabilities at interannual time scales, J. Climate, 24, 5652-5670, 2011.

Pierini, S.: Topographic Rossby modes in the Strait of Sicily, J. Geophys. Res., 101, 6429-6440, 1996.

Pierini, S.: A Kuroshio Extension system model study: decadal chaotic self-sustained oscillations, J. Phys. Oceanogr., 36, 1605-1625, 2006.

Pierini, S.: On the crucial role of basin geometry in double-gyre models of the Kuroshio Extension, J. Phys. Oceanogr., 38, 1327-1333, 2008.

Pierini, S.: Coherence resonance in a double-gyre model of the Kuroshio Extension, J. Phys. Oceanogr., 40, 238-248, 2010.

Pierini, S.: Low-frequency variability, coherence resonance and phase selection in a low-order model of the wind-driven ocean circulation, J. Phys. Oceanogr., 41, 1585-1604, 2011.

Pierini, S.: Stochastic tipping points in climate dynamics, Phys. Rev. E, 85, 027101, 2012.

Pierini, S.: Kuroshio Extension bimodality and the North Pacific Oscillation: a case of intrinsic variability paced by external forcing, J. Climate, 27, 448-454, 2014.

Pierini, S., and Dijkstra, H. A.: Low-frequency variability of the Kuroshio Extension, Nonlin. Proc. Geophys., 16, 665-675, 2009.

Pierini, S., Dijkstra, H. A., and Riccio, A.: A nonlinear theory of the Kuroshio Extension bimodality, J. Phys. Oceanogr., 39, 2212-2229, 2009.

Pierini, S., Fincham, A., Renouard, D., D'Ambrosio, R., and Didelle, H.: Laboratory modeling of topographic Rossby normal modes, Dyn. Atmos. Oceans, 35, 205-225, 2002.

Piola, A. R., and Gordon, A. L.: Intermediate waters in the southwest South Atlantic, Deep Sea Res., 36, 1-16, 1989.

Qiu, B., and Miao, W.: Kuroshio path variations south of Japan: bimodality as a self-sustained internal oscillation, J. Phys. Oceanogr., 30, 2124-2137, 2000.

Quattrocchi, G., Pierini, S., and Dijkstra, H. A.: Intrinsic low-frequency variability of the Gulf Stream, Nonlin. Proc. Geophys., 19, 155-164, 2012.

Rintoul, S. R., Hughes, C., and Olbers, D.: The Antarctic Circumpolar Current System, in “Ocean Circulation and Climate”, Academic Press, 271–302, 2001.

Saraceno, M., Provost, C., Piola, A. R., Bava, J., and Gagliardini, A.: Brazil Malvinas frontal system as seen from 9 years of advanced very high resolution radiometer, J. Geophys. Res., 109, C05027, doi:10.1029/2003JC002127, 2004.

Saraceno, M., Provost, C., and Zajaczkovski, U.: Long-term variation in the anticyclonic ocean circulation over the Zapiola Rise as observed by satellite altimetry: Evidence of possible collapses, Deep-Sea Res., 56, 1077-1092, 2009.

Saraceno, M., and Provost, C.: On eddy polarity distribution in the southwestern Atlantic, Deep-Sea Res. I, 69, 62-69, 2012.

Saunders, P., and King, B. A.: Bottom currents derived from a shipborne ADCP on WOCE cruise A11 in the South Atlantic, J. Phys. Oceanogr., 25, 329-347, 1995.

Schmeits, M. J., and Dijkstra, H. A.: Bimodal behavior of the Kuroshio and the Gulf Stream, J. Phys. Oceanogr., 31, 3435-3456, 2001.

Sgubin, G.: A model study of the Southern Ocean dynamics: mean flow, intrinsic variability and teleconnections, Ph.D. Thesis, University of Naples ”Federico II” and University of Naples "Parthenope", 130 pp., 2012.

Simonnet, E., Ghil, M., and Dijkstra, H. A.: Quasi-homoclinic behavior of the barotropic quasi-geostrophic double-gyre circulation, J. Mar. Res., 63, 931-956, 2005.

Smythe-Wright, D., and Boswell, S.: Abyssal circulation in the Argentine Basin, J. Geophys. Res., 103, 15845-15851, 1998.

Sura, P., Fraedrich, K., and Lunkeit, F.: Regime transitions in a stochastically forced double-gyre model, J. Phys. Oceanogr., 31, 411-426, 2001.

Tai, C.-K., and Fu, L.-L.: 25-day period large-scale oscillations in the Argentine Basin revisited, J. Phys. Oceanogr., 35, 1473-1479, 2005.

Torrence, C., and Compo, G. P.: A practical guide to wavelet analysis, Bull. Amer. Meteor. Soc., 79, 61-78, 1998.

Trenberth, K. E., Olson, J. G., and Large, W. G.: A global ocean wind stress climatology based on ECMWF analyses, NCAR Technical Note NCAR/TN-338, 1989.

Venaille, A., Le Sommer, J., Molines, J.-M., and Barnier, B.: Stochastic variability of oceanic flows above topography anomalies, Geophys. Res. Lett., 38, L16611, 2011.

Volkov, D. L., and Fu, L.-L.: The role of vorticity fluxes in the dynamics of the Zapiola Anticyclone, J. Geophys. Res., 113, C11015, 2008.

Weatherly, G.L.: On deep-current and hydrographic observations from a mudwave region and elsewhere in the Argentine Basin., Deep-Sea Res., 40, 939-961, 1993.

Weijer, W., Vivier, F., Gille, S. T., and Dijkstra, H. A.: Multiple oscillatory modes of the Argentine Basin. Part I: statistical analysis, J. Phys. Oceanogr., 37, 2855–2868, 2007a.

Weijer, W., Vivier, F., Gille, S. T., and Dijkstra, H. A.: Multiple oscillatory modes of the Argentine Basin. Part II: the spectral origin of basin modes. J. Phys. Oceanogr., 37, 2869–2881, 2007b.

Whitworth, T., Nowlin,W. D., Pillsbury, R. D., Moore, M. I., and Weiss, R. F.: Observations of the Antarctic Circumpolar Current and deep boundary current in the southwest Atlantic, J. Geophys. Res., 96, 15105-15118, 1991.

Captions to Figures

Figure 1. Sketch of the upper layer circulation in the southwestern Atlantic (from Saraceno et al., 2004).

Figure 2. Domain of integration and bottom topography.

Figure 3. (a): Steady zonal wind stress profile used to force the circulation model. (b): initial stratifications (red/blue line: temperature profile at the northernmost/southernmost latitude).

Figure 4. Volume transport across the Drake Passage.

Figure 5. (a): Mean SSH (in *m*). (b): Mean depth-integrated currents. (c) Zoom of the current field delimited by the rectangle in panel (b).

Figure 6. Logarithm of the *rms* of the low-frequency SSH signal.

Figure 7. (a): Logarithm of the *rms* of the low-frequency SSH signal in the Argentine Basin. (b): SSH at P1 (the analyses are carried out within the 10-year reference interval delimited by the red lines).

Figure 8. SSH at P1 for the reference interval (black line: total signal; blue line: low-frequency signal). The SSH snapshots corresponding to the green/red dots are shown in Fig. 9.

Figure 9. Snapshots of the low-frequency SSH signal (in *m*) corresponding to the green (column a) and red (column b) dots of Fig. 8.

Figure 10. Upper panels: low-frequency relative vorticity $\tilde{\zeta}$ at t=25000, 27200 days. Lower panel: time series of ζ averaged in sectors A and B for the 10-year reference interval.

Figure 11. Scatter plot of $\tilde{\zeta}$ averaged in sectors A and B.

Figure 12. *Rms* of the high-frequency SSH signal (in *m*) in the Argentine Basin.

Figure 13. (a): Low-frequency SSH at P3 (blue line) and corresponding high-frequency residual (red line) for the reference interval. (b): Wavelet amplitude of the SSH signal for the same point and time interval (the cyan lines indicate the cone of influence).

Figure 14. Snapshot sequence of the SSH high-frequency residual (in *m*) corresponding to a high-frequency maximum of the wavelet amplitude at P3 (see the oval in Fig. 13b).

Figure 15. Green line: Zapiola index. Red and blue lines: integrated wavelet amplitudes $W_{1,50}$ and $W_{100,150}$, respectively.

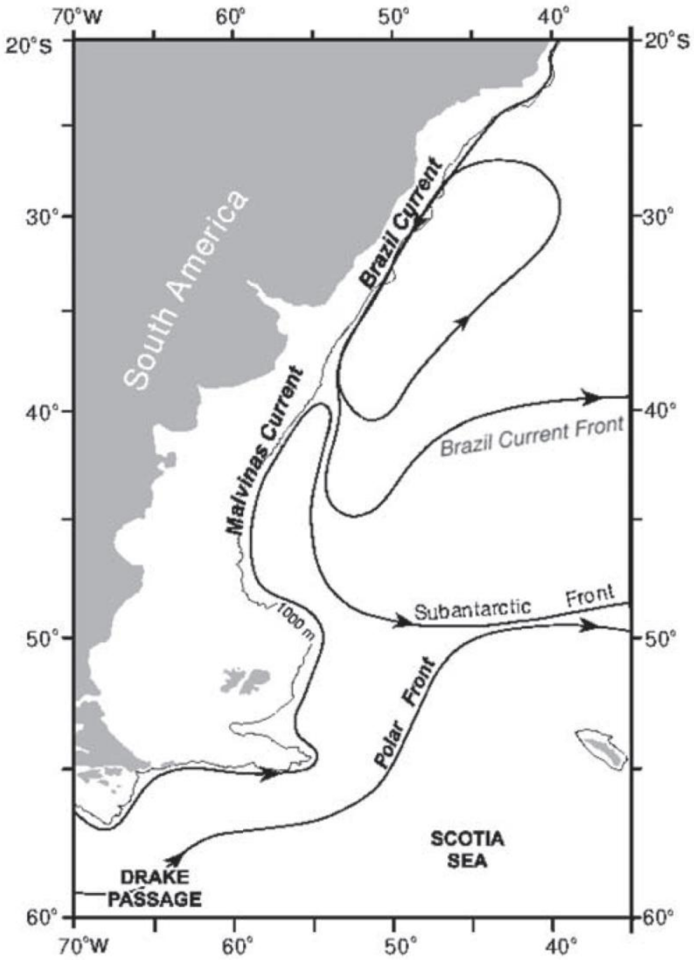

Figure 1. Sketch of the upper layer circulation in the southwestern Atlantic (from Saraceno et al., 2004).

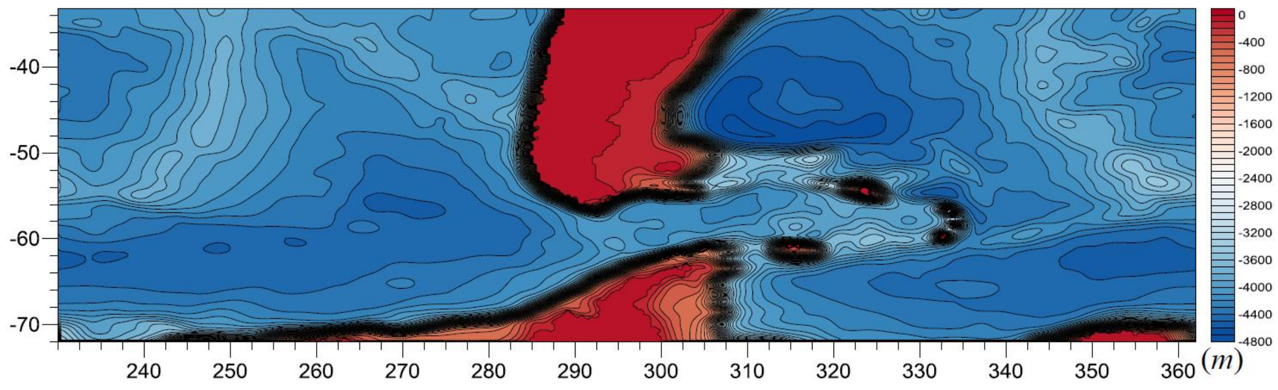

Figure 2. Domain of integration and bottom topography.

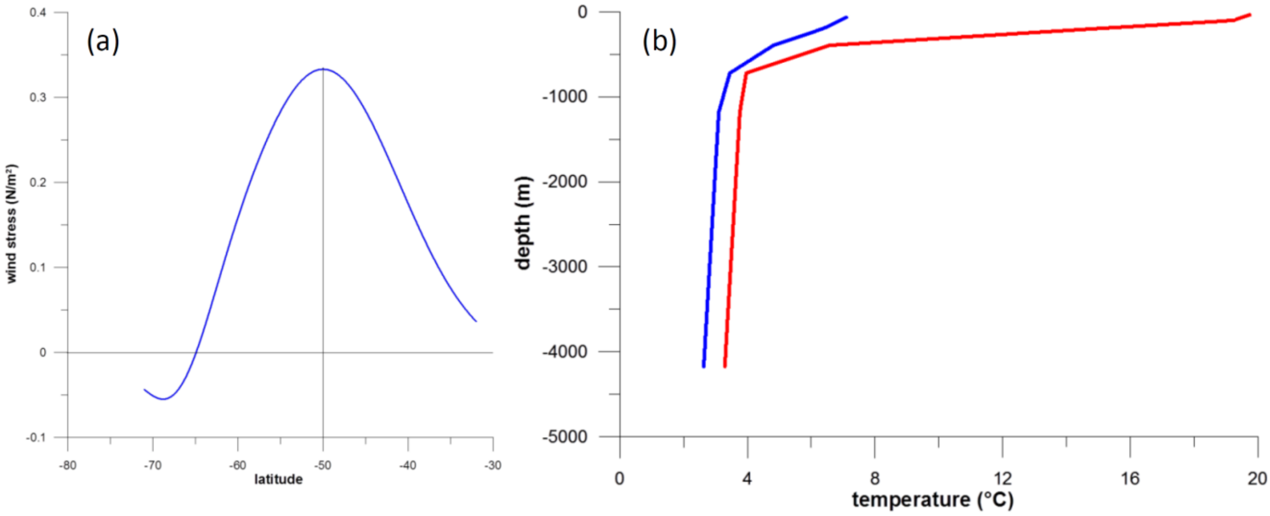

Figure 3. (a): Steady zonal wind stress profile used to force the circulation model. (b): initial stratifications (red/blue line: temperature profile at the northernmost/southernmost latitude).

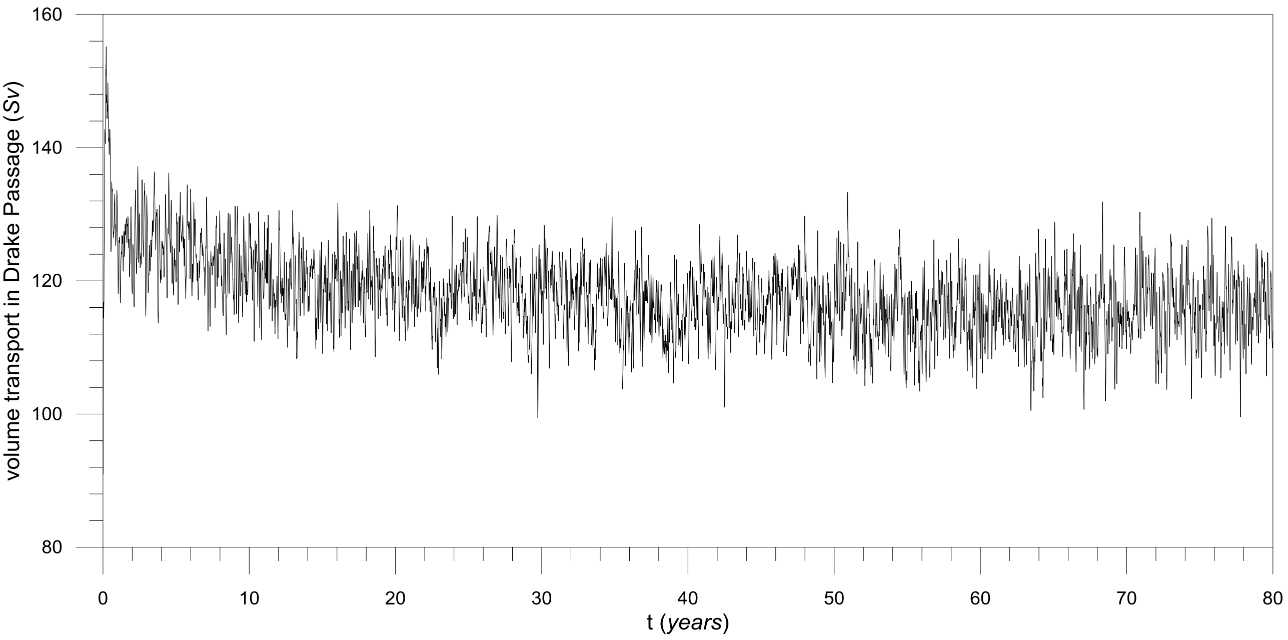

Figure 4. Volume transport across the Drake Passage.

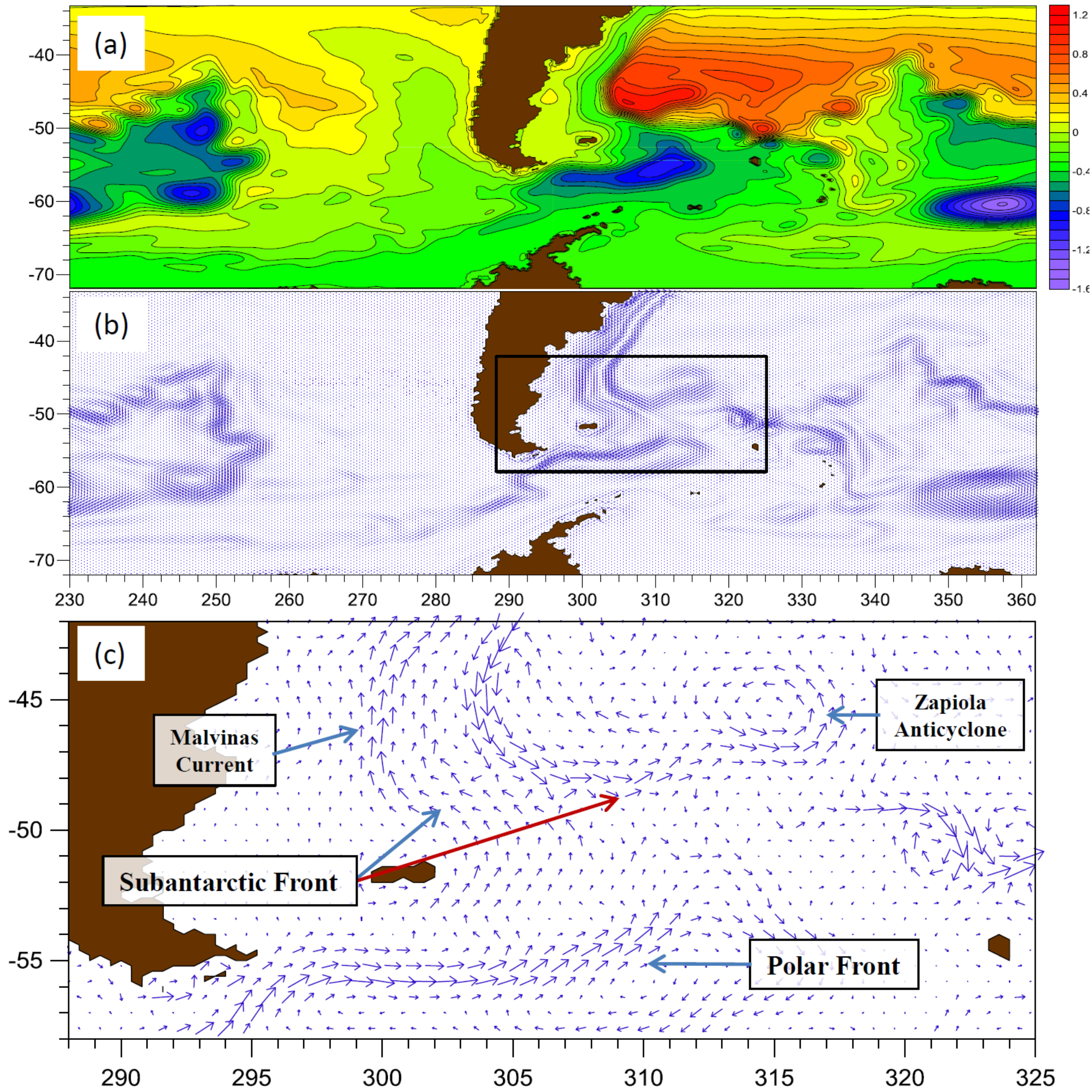

Figure 5. (a): Mean SSH (in *m*). (b): Mean depth-integrated currents. (c) Zoom of the current field delimited by the rectangle in panel (b).

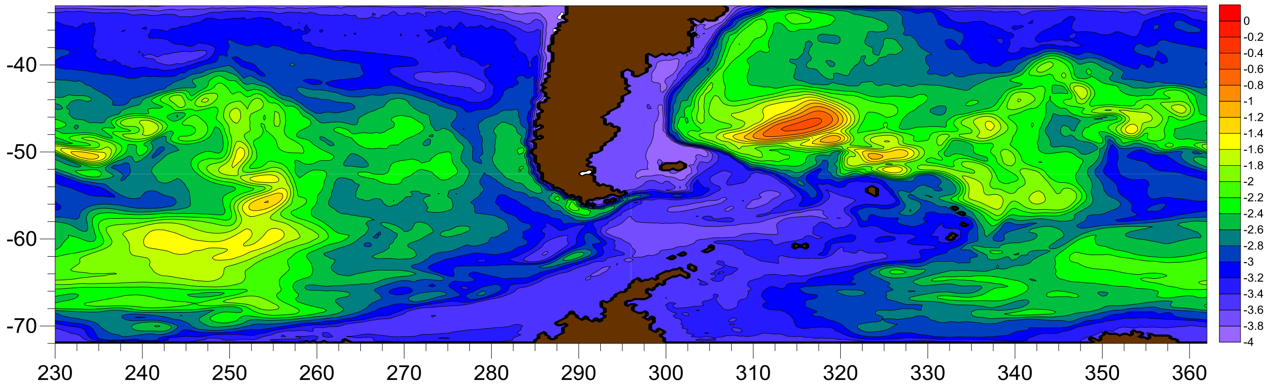

Figure 6. Logarithm of the *rms* of the low-frequency SSH signal.

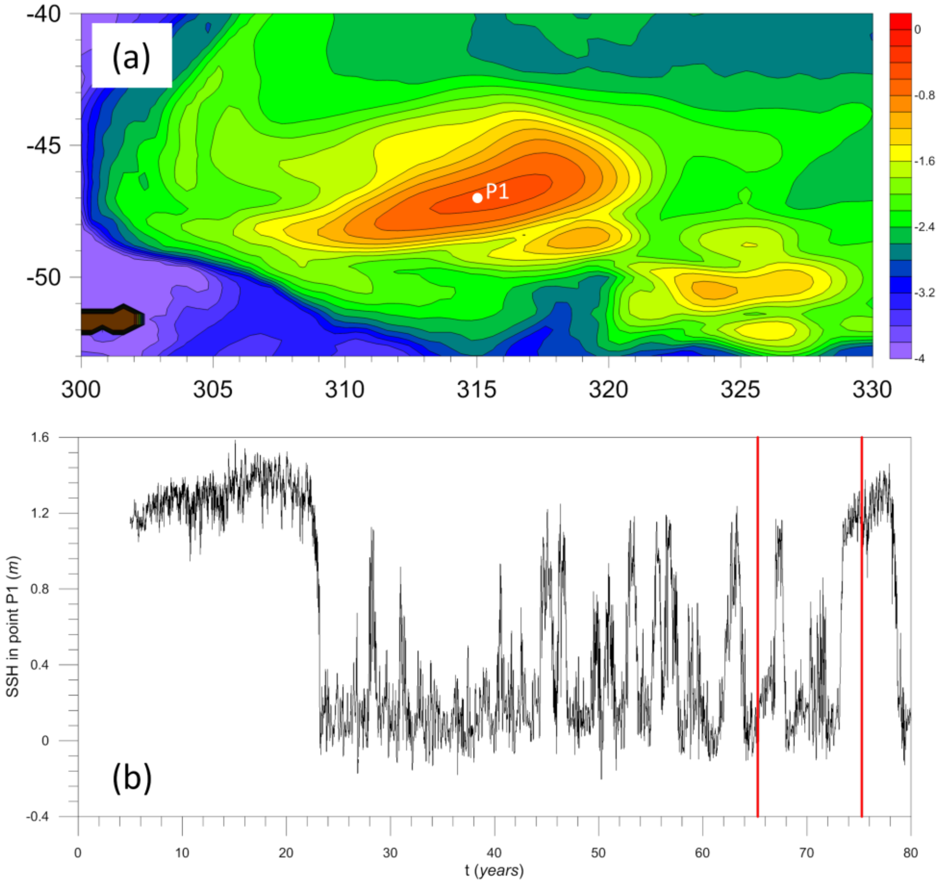

Figure 7. (a): Logarithm of the *rms* of the low-frequency SSH signal in the Argentine Basin. (b): SSH at P1 (the following analyses are carried out within the 10-year reference interval delimited by the red lines).

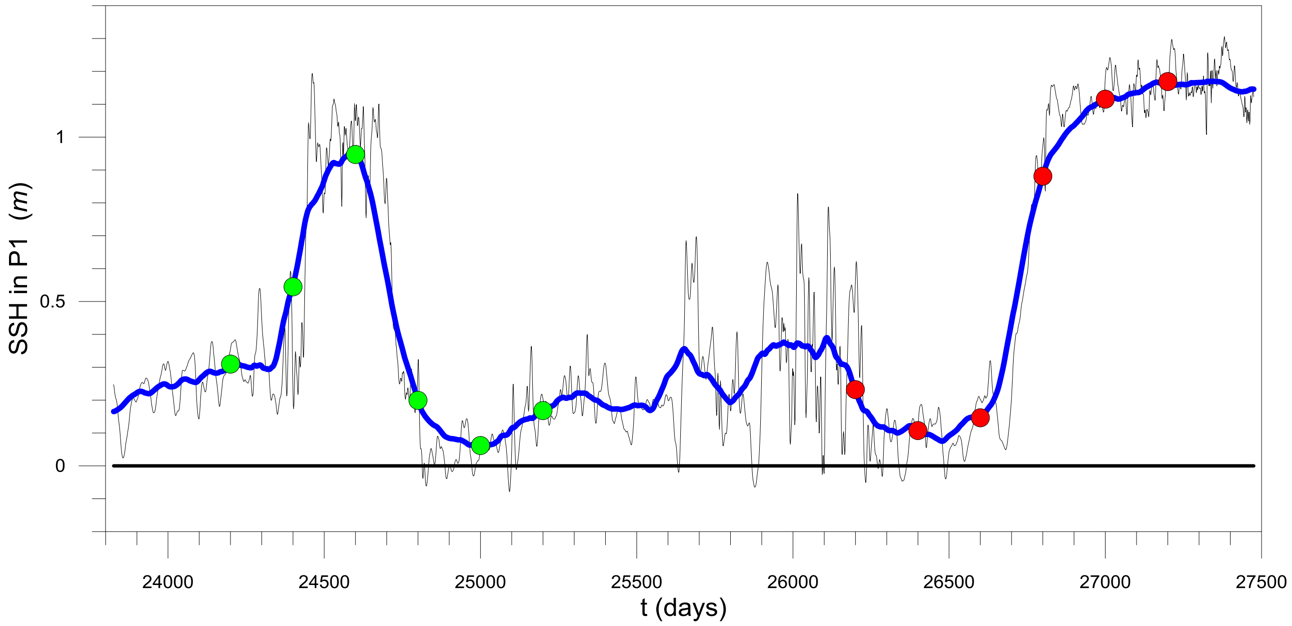

Figure 8. SSH at P1 for the reference interval (black line: total signal; blue line: low-frequency signal). The SSH snapshots corresponding to the green/red dots are shown in Fig. 9.

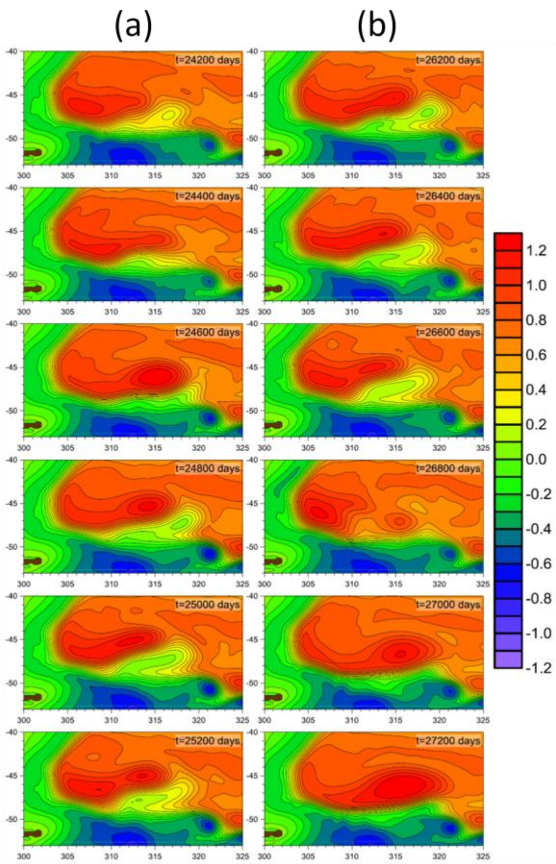

Figure 9. Snapshots of the low-frequency SSH signal (in *m*) corresponding to the green (column a) and red (column b) dots of Fig. 8.

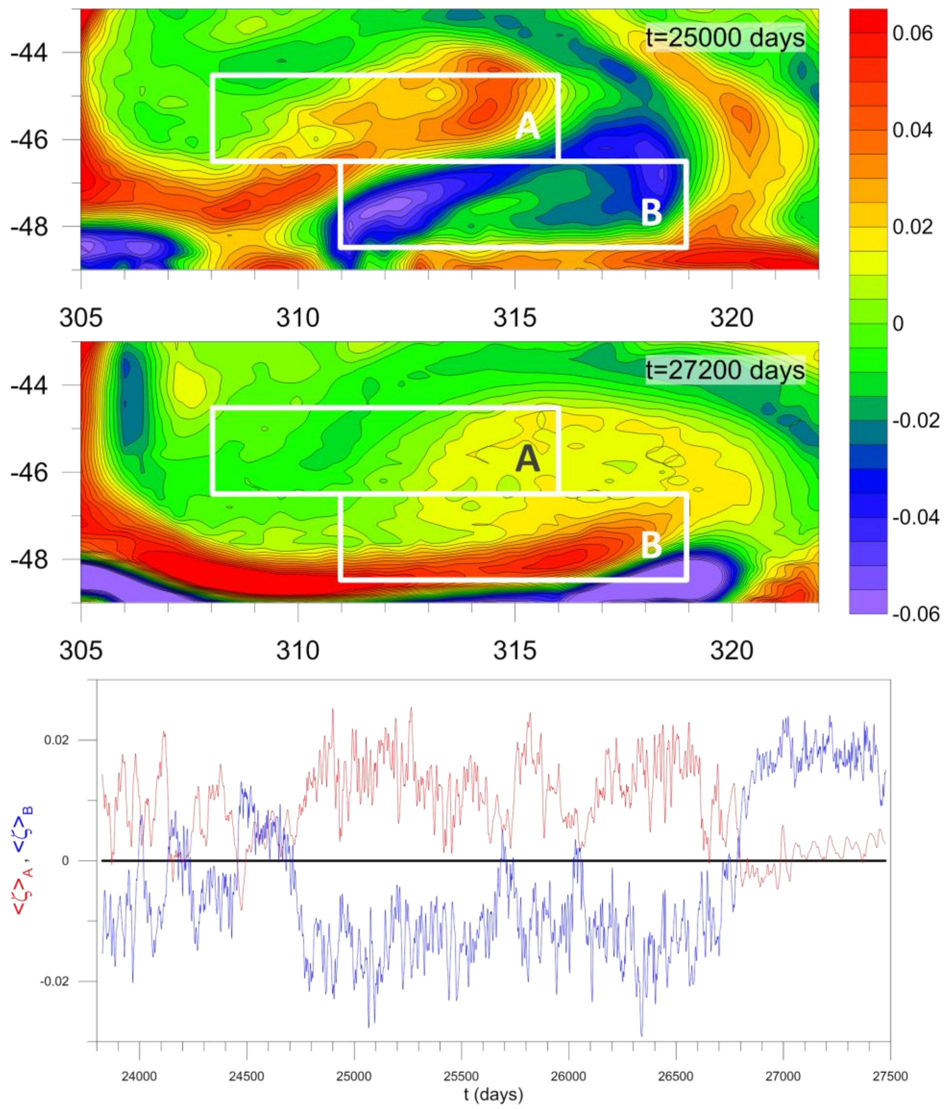

Figure 10. Upper panels: low-frequency relative vorticity $\tilde{\zeta}$ at t=25000, 27200 days. Lower panel: time series of ζ averaged in sectors A and B for the 10-year reference interval.

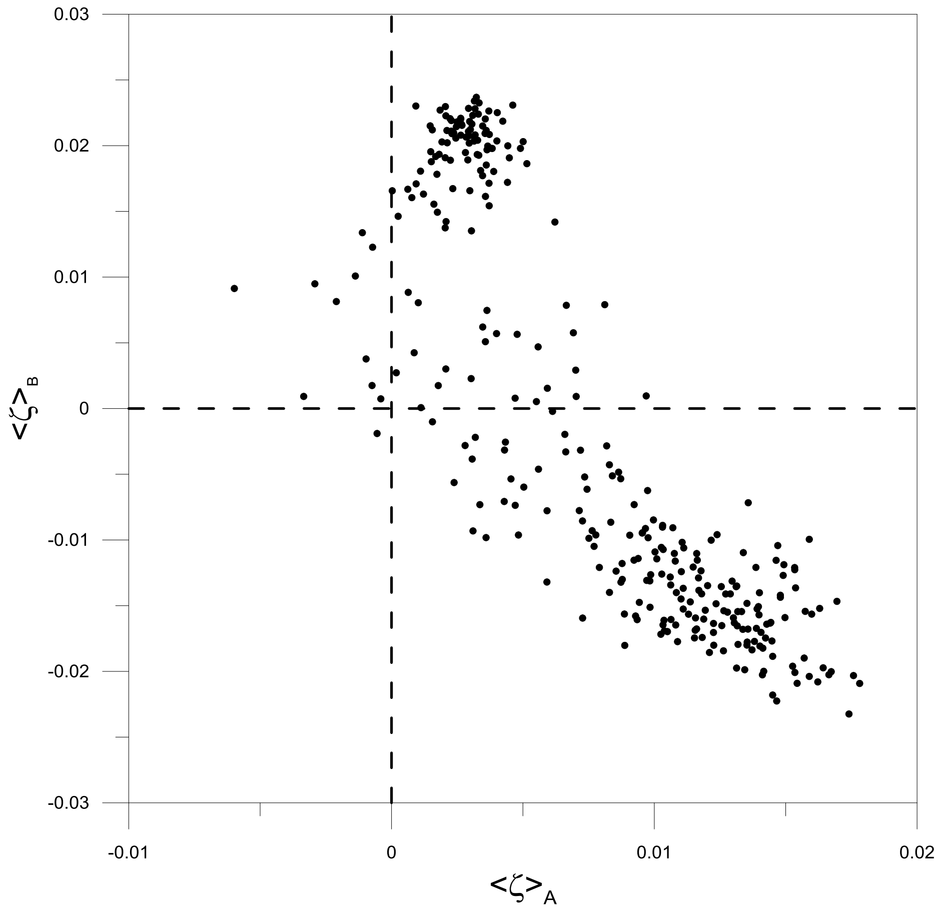

Figure 11. Scatter plot of $\tilde{\zeta}$ averaged in sectors A and B.

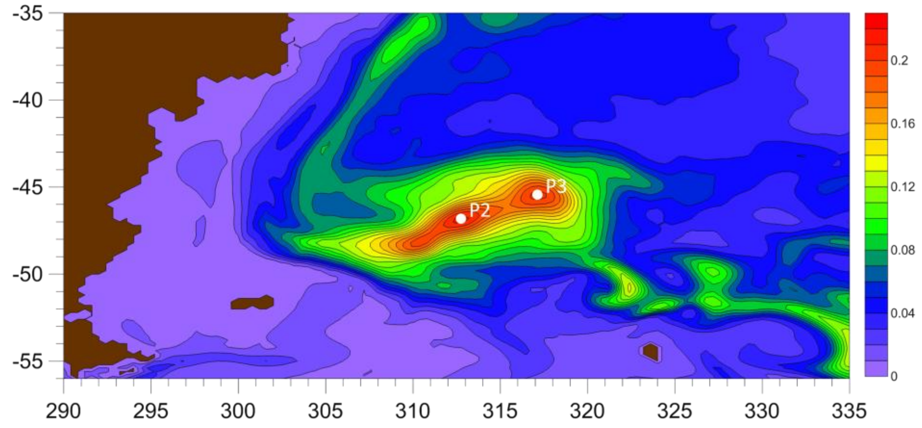

Figure 12. *Rms* of the high-frequency SSH signal (in *m*) in the Argentine Basin.

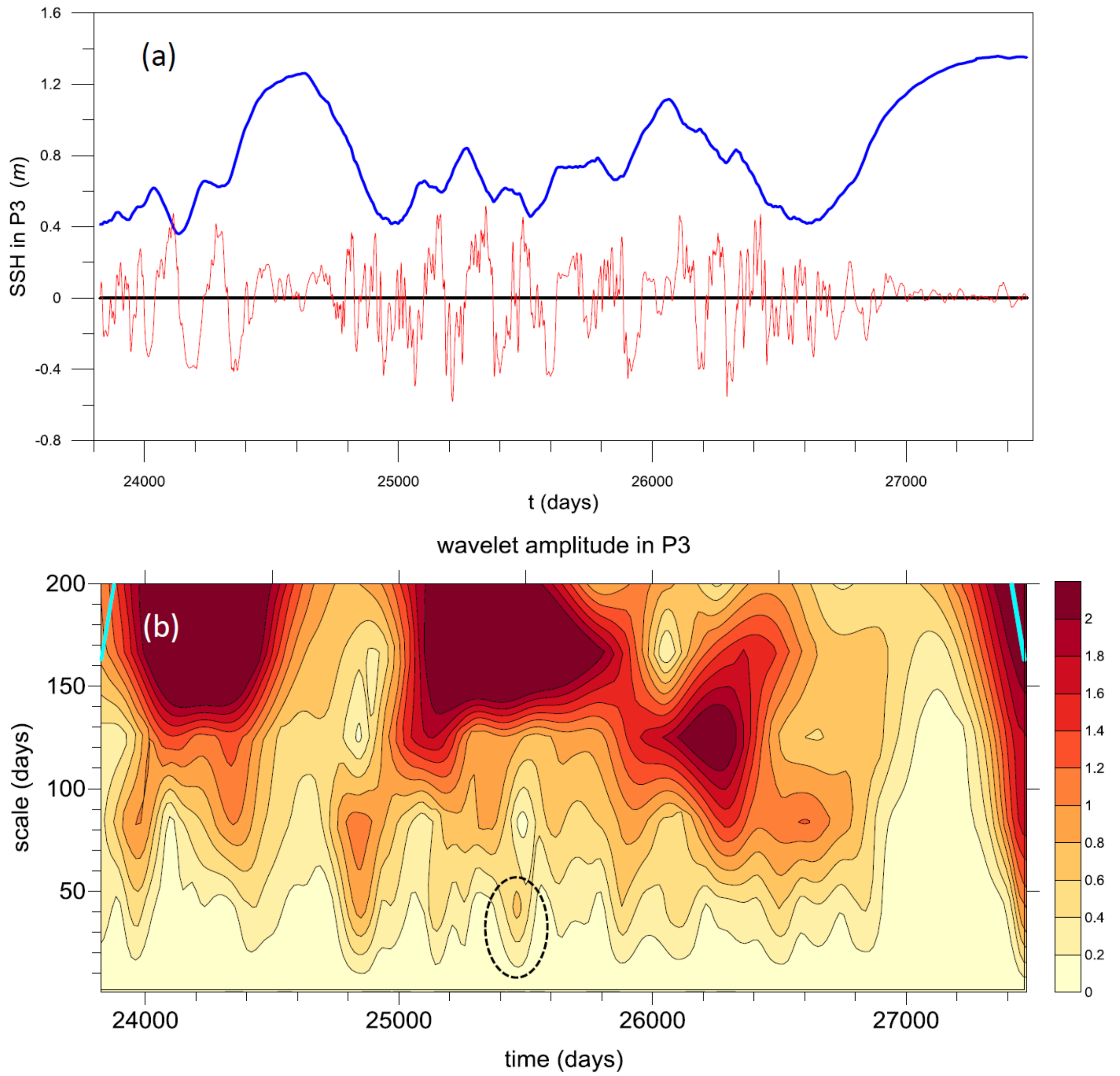

Figure 13. (a): Low-frequency SSH at P3 (blue line) and corresponding high-frequency residual (red line) for the reference interval. (b): Wavelet amplitude of the SSH signal for the same point and time interval (the cyan lines indicate the cone of influence).

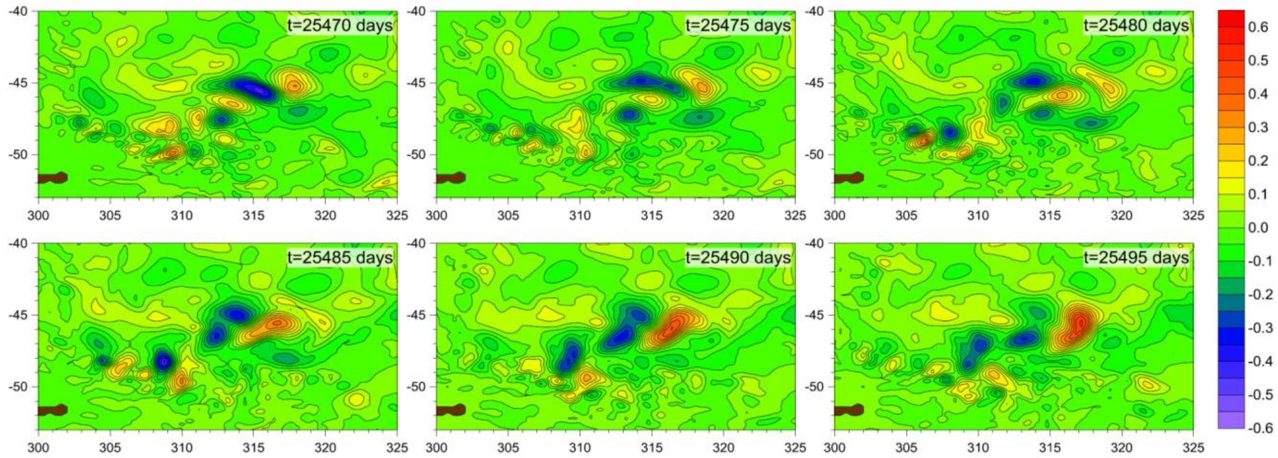

Figure 14. Snapshot sequence of the SSH high-frequency residual (in *m*) corresponding to a high-frequency maximum of the wavelet amplitude at P3 (see the oval in Fig. 13b).

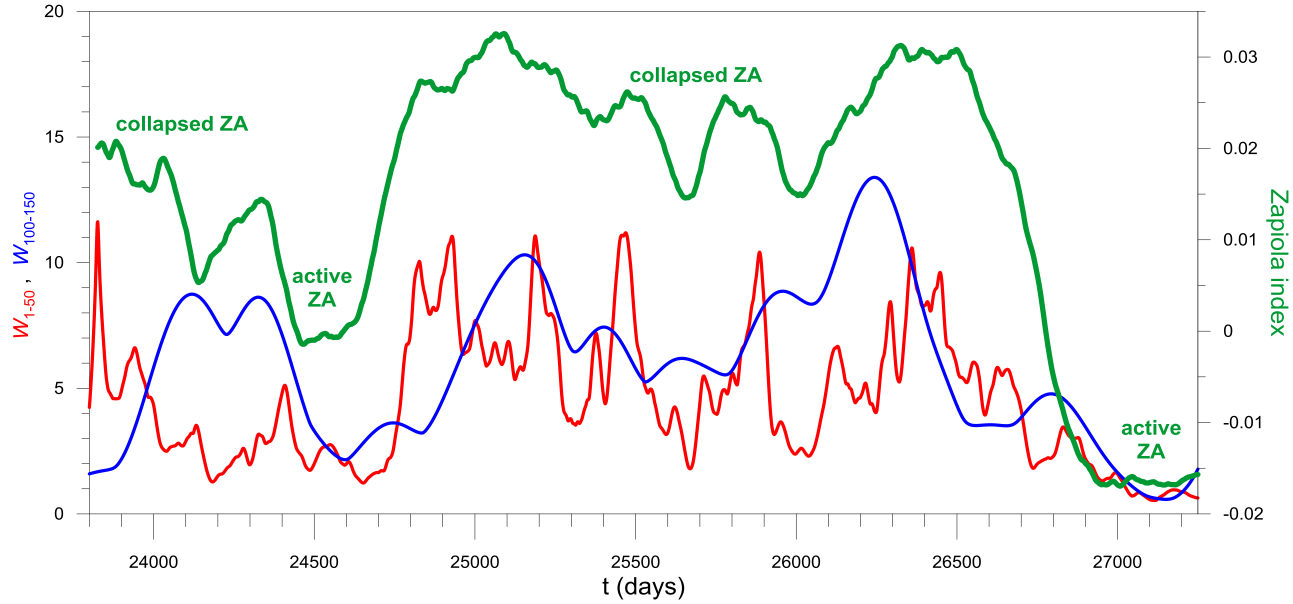

Figure 15. Green line: Zapiola index. Red and blue lines: integrated wavelet amplitudes $W_{1,50}$ and $W_{100,150}$, respectively.